



Spatial Mapping of Dissolved Gases in the Danube Delta Reveals Intense Plant-Mediated Gas Transfer

Marie-Sophie Maier^{1,2*}, Anna R. Canning³, Matthias S. Brennwald⁴, Cristian R. Teodoru^{1,5} and Bernhard Wehrli^{1,2}

¹Institute of Biogeochemistry and Pollutant Dynamics, Department of Environmental Systems Science, ETH Zurich, Zurich, Switzerland, ²Department Surface Waters—Research and Management, Eawag, Swiss Federal Institute of Aquatic Science and Technology, Kastanienbaum, Switzerland, ³GEOMAR Helmholtz-Zentrum für Ozeanforschung Kiel, Kiel, Germany, ⁴Department of Water Resources and Drinking Water, Eawag, Swiss Federal Institute of Aquatic Science and Technology, Dübendorf, Switzerland, ⁵Romanian National Institute of Marine Geology and Geoecology (GeoEcoMar), Bucharest, Romania

OPEN ACCESS

Edited by:

Yves T. Prairie,
Université du Québec à Montréal,
Canada

Reviewed by:

Patrick Höhener,
Aix Marseille Université, France
Núria Catalán,
UMR8212 Laboratoire des Sciences
du Climat et de l'Environnement
(LSCE), France

*Correspondence:

Marie-Sophie Maier
marie-sophie.maier@usys.ethz.ch

Specialty section:

This article was submitted to
Biogeochemical Dynamics,
a section of the journal
Frontiers in Environmental Science

Received: 17 December 2021

Accepted: 14 March 2022

Published: 31 March 2022

Citation:

Maier M-S, Canning AR,
Brennwald MS, Teodoru CR and
Wehrli B (2022) Spatial Mapping of
Dissolved Gases in the Danube Delta
Reveals Intense Plant-Mediated
Gas Transfer.
Front. Environ. Sci. 10:838126.
doi: 10.3389/fenvs.2022.838126

Global estimates see river deltas and estuaries contributing about equally to CO₂ and CH₄ emissions as lakes and reservoirs, despite a factor 6 smaller surface area. Assessing the horizontal gradients in dissolved gas concentrations from large river reaches to connecting canals and wetland lakes remains a challenge in many deltaic systems. To elucidate the processes affecting local CO₂ and CH₄ concentrations in the Romanian part of the Danube Delta, we mapped dissolved O₂, N₂, He and Ar using a portable gas-equilibration membrane-inlet mass spectrometer (GE-MIMS), along with CO₂, CH₄, water temperature and conductivity. We measured the concentrations along the aquatic continuum from a small houseboat during two campaigns, in spring and autumn, to capture different hydrological and plant growth conditions. Delta-scale concentration patterns were comparably stable across seasons. Small connecting channels were highly influenced by the riparian wetland, which was strongest in the eastern part of the biosphere reserve. These sites represented the delta's CO₂ and CH₄ hotspots and showed clear signs of excess air, i.e., supersaturation of dissolved noble gases with respect to air-saturated water. As the adjacent wetland was permanently inundated, this signal was likely caused by root aeration of *Phragmites australis*, as opposed to traditional excess air formation via water table fluctuations in the unsaturated zone. The special vegetation setting with reed growing on floating peat coincided with the highest CO₂ and CH₄ concentrations (>700 μmol/L CO₂ and 13 μmol/L CH₄, respectively) observed in an adjacent channel. Shallow lakes, on the other hand, were major sites of photosynthetic production with O₂ oversaturation reaching up to 150% in spring. The observed deficit in non-reactive gases (He, Ar and N₂) indicated that the lakes were affected by O₂ ebullition from macrophytes. According to our estimations, this ebullitive flux decreased O₂ concentrations by up to 2 mg/L. This study highlights the effect of plant-mediated gas transfer on dissolved gas concentrations and supports recent studies stressing the need to account for ebullitive gas exchange when assessing metabolism parameters from O₂ in shallow, productive settings.

Keywords: carbon cycle, greenhouse gases, noble gases, plant-mediated gas transfer, ebullition, excess air, Danube Delta, membrane-inlet mass spectrometry

1 INTRODUCTION

The release of greenhouse gases from deltaic and estuarine systems cannot be neglected, but the spatial variability of these emissions is poorly understood (Cai, 2011). For CH₄, the most recent global emission estimate from deltas and estuaries is 4.95 TgC year⁻¹ (Borges and Abril, 2011), which equals 25% of the efflux from rivers and streams (0.02 PgC year⁻¹, Stanley et al., 2016). It represents only 3.5–6.3% of the CH₄ flux from lakes and reservoirs (0.139–0.078 PgC year⁻¹, depending on lake size distribution, DelSontro et al., 2018). Global CO₂ emission estimates from deltas and estuaries of 0.27 ± 0.23 PgC year⁻¹ (Laruelle et al., 2010) are only one order of magnitude smaller than the oceanic and terrestrial CO₂ sink (2.5 and 3.4 PgC year⁻¹, Friedlingstein et al., 2020). These estimates are smaller than estimated global CO₂ emissions from rivers (0.48–0.85 PgC year⁻¹, Lauerwald et al., 2015) but in a similar range as emissions from lakes and reservoirs (0.32–0.58 PgC year⁻¹, Raymond et al., 2013; Holgerson and Raymond, 2016). These estimates indicate a very active role of river deltas and estuaries because they exhibit 6 times smaller surface areas when compared to lakes and reservoirs (Laruelle et al., 2010; Holgerson and Raymond, 2016).

The increase of global surface temperatures, its adverse effects for humans and the biosphere (IPCC, 2021), and the potential failure of the Paris agreement (Sachs, 2019) all demand a solid understanding of carbon budgets. In this context, Deemer et al. (2016) identified the lack of adequate spatial coverage as a stumbling block for calculating global greenhouse gas emissions from reservoirs. In contrast to the open ocean or large lakes and rivers, many freshwater systems such as small streams or small lakes can show quite strong horizontal concentration gradients (McGinnis et al., 2016; Natchimuthu et al., 2016). In addition, differences in gas exchange parameters depend on channel slope and morphometry and can change over a small distance (Ulseth et al., 2019; Hall and Ulseth, 2020). The drivers of steep concentration changes can be manifold, ranging from groundwater inflow (Horgby et al., 2019) to changes in depth (Natchimuthu et al., 2016) and hydrodynamics (McGinnis et al., 2016) or organic matter availability (Battin et al., 2008). An additional factor that has so far gained little attention is plant-mediated gas transfer. Recent observations point to oxygen ebullition via photosynthesis (Koschorreck et al., 2017) and other studies suggested specific gas-transfer mechanisms for reed stands, which deserve detailed analysis under field conditions (Brix et al., 1996; Sorrell and Brix, 2013).

River deltas are complex sites, where many of these drivers may govern steep spatial gradients of dissolved (greenhouse) gases across different waterscapes and may introduce large uncertainty to any upscaling approach (Abril and Borges, 2019; Maier et al., 2021). Along with the identification of emission hotspots in single systems, it is therefore vital to understand the processes affecting the spatiotemporal variability of greenhouse gas concentrations in order to improve extrapolation to unsampled territory.

The Danube Delta, Romania, shows very large concentration gradients of dissolved CO₂ and CH₄ with hotspots in some small

channels (Maier et al., 2021). Based on these discrete measurements, steep spatial gradients remain unresolved and potential emission hotspots may be undetected. High-resolution portable sensors measuring dissolved gases such as CO₂ and CH₄ specifically provide a more detailed spatial picture (Canning A. R et al., 2021). Earlier studies showed horizontal gradients in CO₂ and CH₄ concentrations across Danube Delta lakes (Pavel et al., 2009), as well as daily cycles in CH₄ concentrations (Canning A et al., 2021).

While spatial mapping of only CO₂ and CH₄ gives direct indication on the location of potential emission hot spots, measurements of additional gas species can shed further light on the processes that cause or affect these greenhouse gas patterns. Portable membrane-inlet mass spectrometers (MIMS) allow measurements of several dissolved gases in the field (Brennwald et al., 2016) and thus allow to complement greenhouse gas measurements with measurements of noble gases, O₂ and N₂. As noble gases are not affected by biological processes, this allows to get a more detailed view on the physical and biological drivers of the dissolved gas variability. Ar, which has similar solubility characteristics as O₂, is used in oceanography to account for O₂ changes due to physical processes such as waves or degassing (Craig and Hayward, 1987). Recent studies suggest that physical processes like ebullition also play a role in O₂ dynamics in shallow lakes (Koschorreck et al., 2017).

This study builds on a 2-year field campaign at discrete sites in the Danube Delta, which quantified carbon fluxes to the atmosphere (Maier et al., 2021). Here we adopt a same high-resolution mapping approach that allowed Canning A et al. (2021) to identify spatial patterns of methane emissions in the Delta. In order to identify physically and biologically driven gas-transfer mechanisms in more detail, we continuously mapped the spatial distribution of a broad set of dissolved gases (CO₂, CH₄, O₂, N₂, He and Ar) in the Danube Delta. We aimed at 1) identifying spatial patterns and horizontal gradients across the different deltaic waterscapes during two seasons, 2) applying noble gas measurements for constraining physical and biological processes in emission hotspots of greenhouse gases at terrestrial-aquatic boundaries, and 3) quantifying ebullition as a confounding factor in estimates of ecosystem metabolism.

2 MATERIALS AND METHODS

2.1 Study Site

Flowing over 2,850 km and receiving water from 19 different European countries, the Danube River discharges into the Black Sea through a three-arm delta, the Danube Delta. It is Europe's second largest river delta after the Volga wetlands on the Caspian Sea and located at the border of Ukraine to eastern Romania. Runoff from the Carpathian Mountains and the Alps determines the seasonality of the river's hydrology, where peak discharge in spring is followed by low discharge in autumn (**Supplementary Figure S1**). These changes in hydrology directly translate into changes in water level in the delta, leading to flooding of the wetland area in spring and subsequent drainage in autumn.

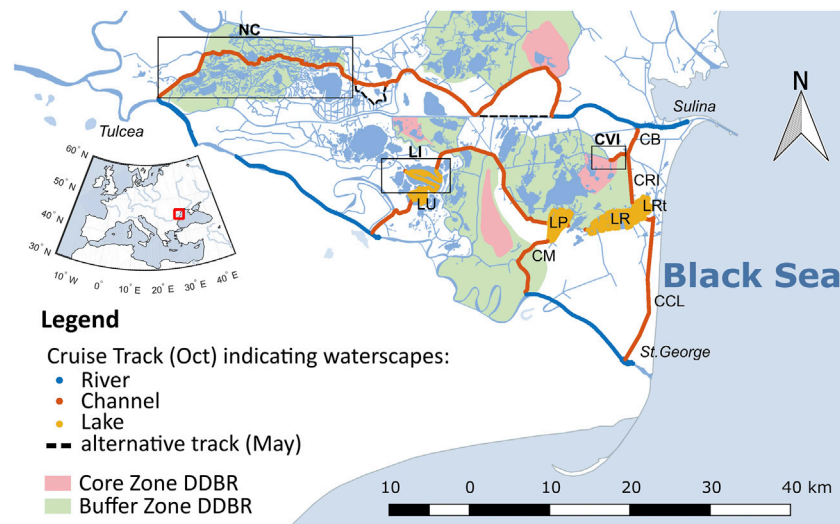


FIGURE 1 | Southern part of the Danube Delta with cruise tracks of the sampling campaign in October 2017. Colors indicate the different waterscapes (blue = river, orange = channel, yellow = lake). The black dotted line indicates where the sampling track in May 2017 differed from October 2017. Red and green areas show the location of core and buffer zones of the Danube Delta Biosphere Reserve (Gastescu, 2013). Boxes indicate specifically discussed sites: NC, northern channels, LI, Lake Isac, CVI, Canal Vatafu-Imputita. Other abbreviations stand for LU, Lake Uzliina (*Lake Isacel*), LP, Lake Puiu, LR, Lake Rosu, LRT, Lake Rosulet, CM, Canal Mocanului (*Canal Mocansca*), CB, Canal Busurca, CRI, Canal Rosu-Imputita, CCL, Canal Cordon Litoral (*Canal Tataru*). Names refer to (Gastescu, 2013), italic names indicate deviating names on maps.google.ch. For mapping details see *Methods* section.

Between the main river branches, the delta consists of vast reed areas and shallow flow-through lakes, which are connected to the main branches via small natural and artificial channels (Figure 1). The river water generally enters the delta at the West and flows back into the river in the East close to the Black Sea. However, depending on the water level fluctuations, direction of flow is also known to reverse in some of the eastern channels (Irimus, 2006). With respect to the 20-years average, the Danube River showed below average discharge throughout most of the monitoring year 2017 (Supplementary Figure S1; ICPDR (2019)).

The Danube Delta is a Ramsar Wetland Site and a World heritage site (UNEP-WCMC (UN Environment Programme World Conservation Monitoring Centre), 2021). Since 1998, it is part of the transboundary UNESCO Biosphere Reserve (UNESCO, 2021). The Danube Delta Biosphere Reserve (DDBR, Figure 1) aims to protect the deltas' diversity of flora and fauna. To this end, about 9% of the deltas' area classifies as strictly protected core zone with another 48% representing buffer zones surrounding the core areas (UNESCO, 2021), where tourism and reed harvesting are restricted.

About 23% of the 220,000 ha reed area represent potential harvesting areas (Covaliov et al., 2010). The reed, predominantly consisting of *Phragmites australis* (Hanganu et al., 2002), is either used as cattle food by locals or professionally harvested by private companies during winter. Burning of the remaining crop parts increases future yield and prevents succession by other plants (Covaliov et al., 2010). Reed grows on reed peat, consisting of a network of viable rhizomes. Initially, this reed peat forms an about 1 m thick floating layer with no contact to the underlying mineral soil. In Romanian, this is called "plaur". Bottom contact

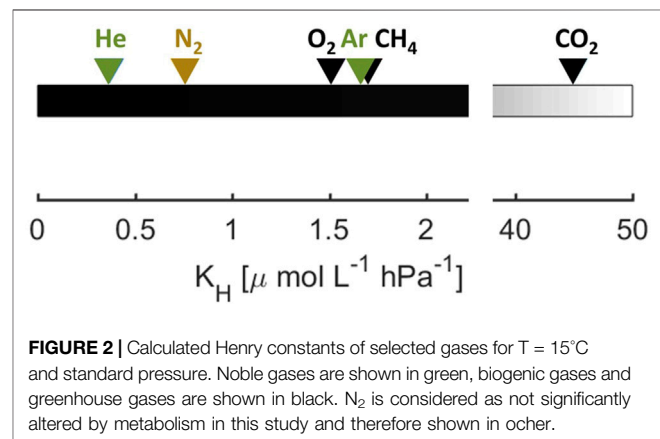


FIGURE 2 | Calculated Henry constants of selected gases for $T = 15^{\circ}\text{C}$ and standard pressure. Noble gases are shown in green, biogenic gases and greenhouse gases are shown in black. N_2 is considered as not significantly altered by metabolism in this study and therefore shown in ochre.

establishes as the peat grows thicker or during low water levels (Hanganu et al., 2002). Both harvesting and burning increases the buoyancy of the plaur and the reed density (Covaliov et al., 2010), yet reduce the abundance of old and broken reed culms, which play an important role in oxygenating the rhizome (Sorrell and Brix, 2013).

As road infrastructure through the delta is lacking, ships and boats are the most important means of transport there. This boat traffic likely enhances gas exchange in some of the small, highly frequented channels, as well as in the main branches.

2.2 Measured Gas Species

For this study, we complemented CO_2 and CH_4 measurements with measurements of dissolved noble gases (He and Ar), O_2 and N_2 . Noble gases such as He and Ar help to understand the

physical changes affecting all dissolved gas concentrations. As most poorly soluble gas in the water (**Figure 2**), He is affected most strongly by gas bubbles rising through the water column. On their way through to the surface, less soluble gases from the surrounding water replace more soluble gases initially present in the bubble (McGinnis et al., 2006), which is called stripping. We expected to see such a stripping effect for He during ebullition, i.e., enhanced gas transfer to the atmosphere via bubbles.

The solubility properties of Ar are very similar to those of O₂ and comparable to N₂ (about 2:1). It is therefore often used to account for physical changes affecting these gases or to improve measurement accuracy by employing O₂:Ar or N₂:Ar ratios (Craig and Hayward, 1987; Groffman et al., 2006). O₂:Ar ratios are frequently used in the ocean for quantifying net community production (Craig and Hayward, 1987; Tortell et al., 2015) but also in ice cores (Zhou et al., 2014).

In combination, noble gases can indicate the presence of excess air, i.e., an observed surplus of dissolved gas in excess to atmospheric equilibrium concentrations with air-like gas composition (Heaton and Vogel, 1981). This phenomenon is traditionally observed in unconfined groundwater bodies, where air entrapment during a rising groundwater table leads to an increase in hydraulic pressure, allowing the water to take up more gas and thus partially or fully dissolving the trapped gas bubble (Aeschbach-Hertig et al., 1999). This presence of excess air can raise the O₂ and N₂ saturation beyond expectation in river banks and groundwater (Mächler et al., 2013).

The concentration of O₂ represents an indicator for the ecosystem metabolism, i.e., autotrophic versus net heterotrophic conditions. *In-situ* O₂ concentrations are often used as a measure for net primary productivity, i.e., primary production–respiration. Different methods include the measurement of diel O₂ changes in streams and lakes (Staehr et al., 2012; Hall et al., 2016; Bernhardt et al., 2018).

Since our measurement system was not sensitive enough to resolve small biogenic changes in N₂ from the comparably large N₂ background concentration of air-saturated water, we used molecular nitrogen as a third conservative gas species in this study.

2.3 Sampling

We continuously measured the concentrations of dissolved gases (CO₂, CH₄, He, Ar, O₂, N₂) in the southern part of the Danube Delta during two field campaigns in May and October 2017. The journey of our sensor-equipped houseboat covered the different waterscapes of the delta, i.e., main river branches, small channels and large flow-through lakes (**Figure 1**). The size of our houseboat prevented accessibility of shallower lakes or narrower channels (**Supplementary Figure S2**). Due to time constraints, the paths in May and October deviate slightly in the northern part of the mapping area.

For the analysis of dissolved He, Ar, O₂ and N₂, we used a membrane-inlet mass spectrometer (MIMS) from Gasometrix (Brennwald et al., 2016) in combination with a submersible pump and a membrane-equilibrator. The total number of datapoints per gas species amounted to ~8,600 in May and ~8,900 in October. We filled gasbags with a known composition of pressurized air

enriched with CO₂ and CH₄ and used those as standard gas mixture during the field trip. This standard gas and ambient air were measured in regular intervals (every fifth and 10th sample batch, respectively, with 1 sample batch representing five individual measurements) to ensure data accuracy. The partial pressures and concentrations of the gases dissolved in water were quantified from the raw MIMS data following the procedures described in Brennwald et al. (2016). Given the large concentration gradients in the delta, we performed the calculations for individual measurements. Where necessary, e.g., to compare gases measured by different detectors, averages and standard deviations were calculated for the closest five measurements (i.e., 1 sample batch). Standard/ambient air measurements were performed along the journey, therefore introducing regular gaps in the dissolved concentration maps. Ambient air measurements of He, Ar, N₂ and O₂ were processed the same way as other samples and used as quality control. The standard deviation varied <1.7% for Ar and O₂, ~0.5% for N₂ and <7% for He. Average ambient air measurements were up to about 2% (N₂, Ar, O₂) or 3.5% (He) smaller than global values (see **Supplementary Table S1**).

In addition to the MIMS, we used a set-up with combined flow-through sensors, which included CONTROS HydroC[®] CO₂ FT and CONTROS HydroC[®] CH₄ FT sensors (formerly Kongsberg Maritime Contros GmbH, Kiel, Germany; now -4H- JENA Engineering GmbH, Jena, Germany) to measure CO₂, and CH₄, respectively. The setup also included a SBE 45 micro thermosalinograph (Sea-Bird Scientific, Bellevue, WA, United States) to measure temperature and conductivity on-board. For details please refer to Canning A. R et al. (2021). This part of the data is available via the Pangaea database (Canning et al., 2020) and details on CH₄ concentrations were previously published by Canning A et al. (2021). We recorded GPS position, depth and *in-situ* temperature with a Lowrance HDS5 sonar.

2.4 Data Analysis

2.4.1 Calculation of Saturation Concentrations

We calculated the saturation concentrations for the different gas species according to the temperature-salinity-solubility relations for He (Weiss, 1971), O₂ (Garcia and Gordon, 1992), N₂ and Ar (Hamme and Emerson, 2004), CO₂ (Weiss, 1974) and CH₄ (Wiesenburg and Guinasso Jr, 1979). For the actual partial pressure in the atmosphere, we used 400 ppm for CO₂ and 1,840 ppb for CH₄. Since we are working in freshwater, we set salinity to 0 for the calculations. A comparison of the Henry coefficients at 15°C and standard pressure shows that He is the least soluble of the investigated gases (**Figure 2**), followed by N₂, while O₂, Ar and CH₄ have very similar solubility, and CO₂ is the most soluble gas by far.

2.4.2 Classification Into Waterscapes and Definition of Striking Sites

In the data analysis, we took a closer look at the three different waterscapes, i.e., river, channel and lakes (**Figure 1**) that were classified as specified in Maier et al. (2021). In brief, the main branches of the River Danube belong to the river class, while old

cut-off meanders and small channels with a low flow velocity are defined as channels. The lake class includes the shallow delta lakes. In addition to these three waterscapes, we evaluated three sites, where we found extreme values of dissolved gas concentrations: Lake Isac, Canal Vatafu-Imputita and a combination of channels in the north (see boxes in **Figure 1**). These sites are representative of different areas within the delta with prominent characteristics.

The northern channels cut through the Sontea-Fortuna lake complex in the north of the delta and include Canal Mila 35, Canal Sontea and Garla Sontea (Gastescu, 2013). Especially in the western-most part of the northern channel complex, the canals are bordered by river levees (**Supplementary Figure S8**). The vegetation is a mix of natural floodplain forest, mixed reed mace and pure reed vegetation on mineral and organic soils. In some places, the river levees are used for wood extraction, cattle grazing and small vegetable gardens (Hanganu et al., 2002). These channels are representative for most small channels in this area.

Canal Vatafu-Imputita is situated in the Rosu-Puiu complex in the eastern part of the delta (Oosterberg et al., 2000) at the border of the Vatafu-Lungulet core protection zone and the surrounding buffer zone. This area is situated in a depression zone and lies below sea level (Gastescu, 2013). As a result, the area is permanently inundated (**Supplementary Figure S8**). The dominant vegetation is reed, which mainly occurs on plaur. However at the Easternend of the channel also “mineral soils” and “salinized soils” occur (Hanganu et al., 2002), which may reflect the evolution of the delta over time (Panin, 1996). Judging from vegetation and elevation maps, the channels in the Matita-Merhei lake complex in the North shows similar characteristics (Hanganu et al., 2002; Gastescu, 2013).

Lake Isac belongs to the Gorgova-Uzlina lake complex in the fluvial part of the delta and has a residence time of about 12 days (Oosterberg et al., 2000). With about 10.2 km² it is the deltas' fourth largest lake with respect to open water surface area and has an average water depth of 2.4 m (Oosterberg et al., 2000). It was categorized as large and turbid lake by Oosterberg et al. (2000) and as “intermediate” type lake showing “a combination of clear water, submerged vegetation, suspended solids and algal blooming” by Coops et al. (1999). This matches our recent observations, where Lake Isac had abundant submerged vegetation in spring and early summer, while later in the year it showed signs of an algal bloom (Maier et al., 2021). Examples of lakes in the delta showing similar characteristics are Lake Fortuna and Lake Gorgova (Coops et al., 1999). Apart from Lake Isac, the other mapped lakes were classified as “turbid” with less abundant submerged vegetation (Coops et al., 1999; Oosterberg et al., 2000).

2.4.3 Estimation of Excess Air and Equilibration Temperature

To estimate the excess air present in our system, we used both a visual approach for three of the locations, where enough data was present, as well as the “nobelfit”-routine (Brennwald, 2020).

For the visual approach, which is helpful to understand the concept of excess air, we plotted He concentrations against Ar concentrations in ccSTP/g (cubic centimeters at standard conditions per mass of water, 1 ccSTP = 1/22,414 Mol). We

included the line that represents air saturated water samples (ASW) equilibrated at different temperatures, as well as a line indicating the concentration changes of ASW when excess air, A , increases at a certain temperature, T_w .

The unfractionated excess air model (UA-model) is the simplest concept to describe the excess air phenomenon. It assumes complete dissolution of an entrapped air bubble as described by:

$$C_i = C_i^{ASW}(T_w, p) + A \cdot z_i \quad (1)$$

where C_i is the dissolved gas concentration of species i . C_i^{ASW} is the concentration in water in equilibrium with air (air saturated water), which is a function of the equilibration temperature, T_w and ambient pressure, p . The factor z_i refers to the volume fraction in dry air of the respective gas i and A denotes the initially entrapped amount of dry air per unit mass of water (Aeschbach-Hertig et al., 2008).

Using the script “nobelfit.m” (Brennwald, 2020), which is based on a χ^2 regression model, we employed He, Ar and N₂ as tracers to solve **Eq. 1** for A and T_w . While a positive A -value indicates a surplus of gas dissolved in the water, a negative A -value can be interpreted as a sign for degassing, e.g., by gas stripping via ebullition.

Since He concentrations in our system are likely affected by ebullition, we also used traditional O₂:Ar ratios to disentangle the biologically produced amount of O₂ from physical changes in dissolved gas saturations.

2.4.4 O₂ Estimation From O₂:Ar Ratio

Given their similar solubility (**Figure 2**), O₂ and Ar concentrations are affected in a similar way by physical changes, such as changes in temperature and pressure or gas stripping. Biological processes, i.e., O₂ production or consumption via photosynthesis or respiration, on the other hand do not affect Ar concentrations, thereby creating a difference in the O₂:Ar ratio. In environments where ebullition or air entrapment play a large role and in the absence of other Ar sources or sinks, the O₂:Ar ratio can be used to disentangle the biologically induced O₂ changes from physical changes (Craig and Hayward, 1987).

We calculated $\Delta O_2/Ar$, the biologically induced disequilibrium of O₂ with respect to Ar from the O₂ and Ar saturation ($O_{2,sat}$, Ar_{sat}) by rearranging the equation used by Zhou et al. (2014):

$$\Delta O_2/Ar = \frac{[O_2]/[Ar]}{[O_2]_{eq}/[Ar]_{eq}} - 1 = \frac{[O_2]/[O_2]_{eq}}{[Ar]/[Ar]_{eq}} - 1 = \frac{O_{2,sat}}{Ar_{sat}} - 1, \quad (2)$$

where $[O_2]$ and $[Ar]$ are the measured concentrations and $[O_2]_{eq}$ and $[Ar]_{eq}$ denote the concentrations in air equilibrated water.

The amount of O₂ associated to biological activity thus follows as:

$$[O_2]_{bio} = \Delta O_2/Ar \cdot [O_2]_{eq} \quad (3)$$

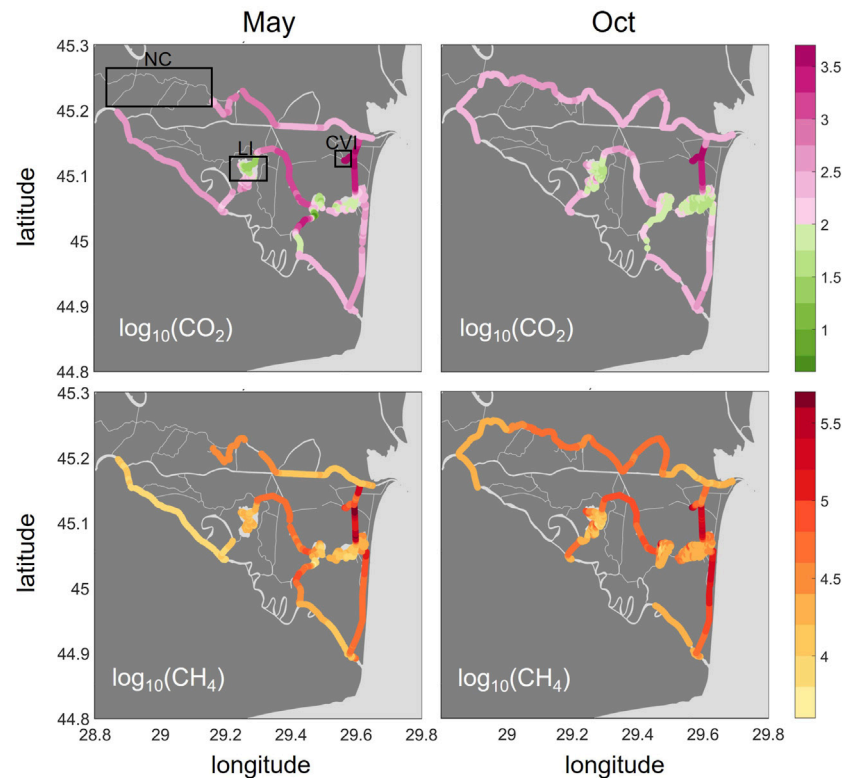


FIGURE 3 | Spatial distribution of greenhouse gas saturations (%) as CO₂ (top row) and CH₄ (bottom row) in May and October 2017 presented as log₁₀ (). Color coding: pink for CO₂ represents oversaturation (>2), green indicates undersaturation. CH₄ is oversaturated throughout the delta. The boxes in the upper left graph indicate the locations of the Northern Channels (NC), Lake Isac (LI) and Canal Vatafu-Imputita (CVI). The two plots for CH₄ were adapted from Canning A et al. (2021).

and can be either positive (photosynthesis) or negative (respiration). We calculated the difference between the measured O₂ concentration and the concentration expected from the O₂:Ar ratio by adding the biological O₂ to the equilibration concentration:

$$[\text{O}_2]_{\text{dif}} = [\text{O}_2]_{\text{meas}} - ([\text{O}_2]_{\text{bio}} + [\text{O}_2]_{\text{eq}}) \quad (4)$$

Negative [O₂]_{dif} implies that O₂ is missing with respect to what we would expect at Ar saturations of 100%.

2.4.5 Spatial Maps and Statistical Analysis

We used Matlab R2017a and R2017b to create the figures and conduct statistical analyses. For the spatial maps, we updated publicly available shape files for Romania and Ukraine (Mapcruzin, 2016; <https://mapcruzin.com/>, last access: 13 December 2016) using the OpenLayers plugin in QGIS. This data sources contains information from openstreetmap.org, which is made available under the Open Database License (ODbL) at <https://opendatacommons.org/licenses/odbl/1.0/>. To compare the concentrations and saturations in the three different waterscapes and three additional sites of interest, we used the “distributionPlot.m” function (Jonas, 2021). Source code from the “noblefit”-package (Brennwald, 2020) was run on GNU Octave (version 4.2.1).

3 RESULTS

3.1 Dissolved Greenhouse Gases: CO₂ and CH₄

Both CO₂ and CH₄ showed very large concentration ranges and steep gradients across the delta with a hotspot area in the East that persisted across seasons (Figure 3). As the green colors indicate, CO₂ was undersaturated in many parts of the lakes in both seasons with a median across all lakes of 96% saturation in May and 65% in October. We encountered exceptions for the western lake areas close to the inflow, which receive water from wetlands and channels. These channels, as well as the river main branches, were oversaturated in CO₂ across seasons (median in May and October: 279 and 283%, respectively, in the river branches and 1,270%, respectively, 270% in the channels). Compared to the river reaches, the oversaturation in the channels showed a larger range (Supplementary Table S3). The highest concentrations were found in Canal Vatafu-Imputita (median: 3,000% and 4,400% in May and October, respectively, Supplementary Table S4) and the adjoining channels, Canal Busurca (leading north) and Canal Rosu-Imputita (leading south to Lake Rosu, Figure 1). While Canal Busurca showed high concentrations along the whole

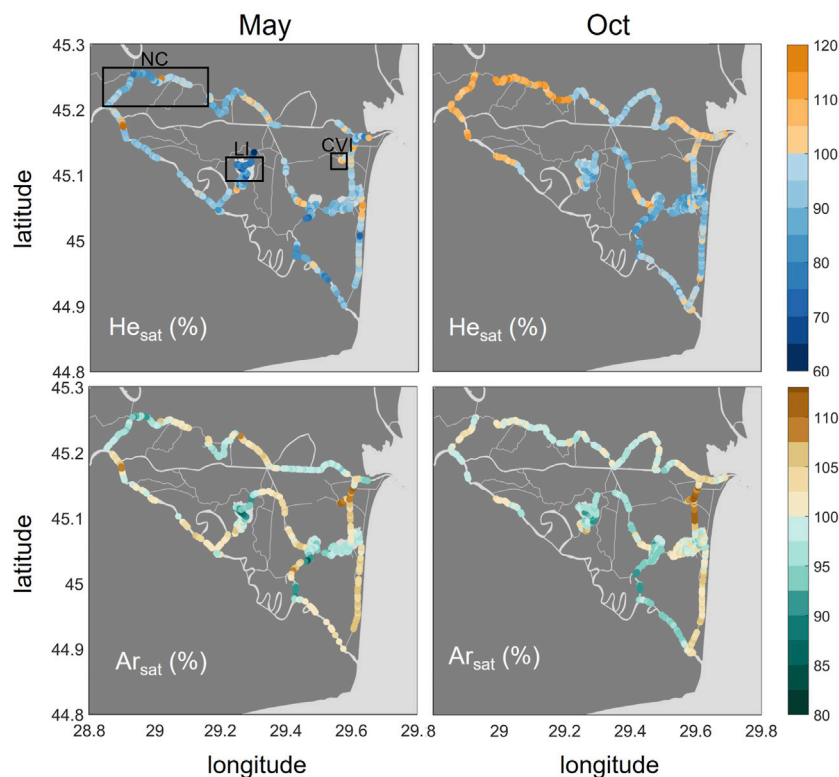


FIGURE 4 | Spatial distribution of He (top row) and Ar (bottom row) in % saturation in May and October 2017. Oversaturation is shown in orange/brown and undersaturation in blue/turquoise. Please note the different ranges of the color bars. The boxes in the upper left graph indicate the locations of the Northern Channels (NC), Lake Isac (LI) and Canal Vatafu-Imputita (CVI).

channel stretch in May, concentration dropped along the channel in October, indicating the reversal of flow direction along the first part of the channel.

CH₄ was oversaturated in all parts of the delta, with the lowest saturations occurring in the main branches of the Danube (median: 10,700 and 18,000% in May and October, **Figure 3** and **Supplementary Table S3**) followed by the lakes (median: 16,600 and 22,300% in May and October, respectively). Channels showed the highest CH₄ saturations (median: 41,200 and 57,700% in May and October, respectively). In contrast to CO₂, the highest CH₄ saturations were not found in Canal Vatafu-Imputita directly, but rather in Canal Rosu-Imputita. Canal Cordon-Litoral showed elevated CH₄ partial pressures that covered a long stretch especially in October. CO₂ was only mildly oversaturated in this channel.

3.2 Noble Gases: He and Ar

The noble gases, He and Ar (**Figure 4**), generally showed undersaturation conditions in lakes, with the strongest undersaturation occurring in Lake Isac for both gases in May (median: 77 and 91%, respectively). The strongest oversaturation, in contrast, was found in small channels. While the highest He saturations were observed in the Northern Channels in October (median: 108%), the eastern channels around Canal Vatafu-Imputita showed the maximum Ar saturations in both seasons

(median: 108% in May and 112% in October). Along the stretch of this channel, we observed both under and oversaturated conditions with respect to He.

3.3 O₂ and N₂

O₂ saturations covered a large range from 19% to 162% in May and 5.2% to 139% in October (**Figure 5**). The main river branches were slightly undersaturated in both seasons with a median of 90 and 92% in May and October, respectively. In contrast to the other gases, O₂ saturations were highest in the lakes, especially in Lake Isac (median: 147% in May). The CO₂ hotspot, Canal Vatafu-Imputita, had the lowest O₂ saturations. The saturations were as low as 19% in May and 5% in October at that spot and adjoining channels, which is less than 2 mg/L and therefore too low for the survival of most fish species.

The N₂ saturations we observed ranged between 74 and 111% in May and 87–108% in October (**Figure 5**). N₂ was generally undersaturated in the lakes, while some of the channels showed oversaturation. N₂ saturations were elevated in the channels downstream of small settlements and lodging houses, for example in the channel leading from the main river to Lake Uzlina (Canal Uzlina) and the channel entering Lake Puiu from the west (Canal Caraorman). The strongest oversaturation in both May and October (median: 109 and 108%, respectively) was found in the CO₂ hotspot, Canal Vatafu-Imputita.

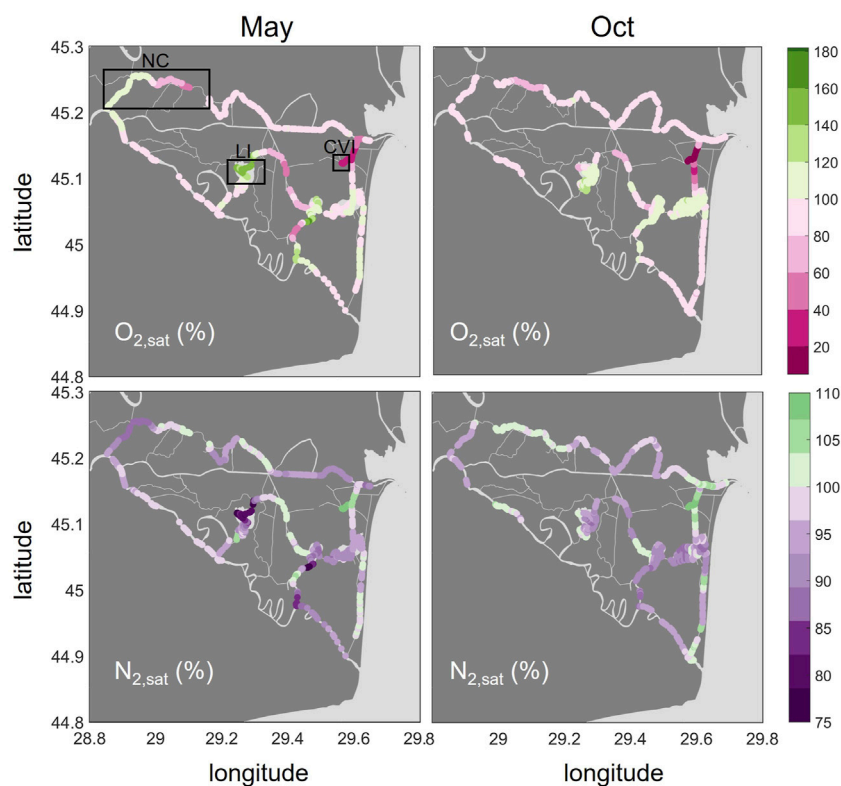


FIGURE 5 | Spatial distribution of O_2 (top row) and N_2 (bottom row) in % saturations in May and October 2017. Oversaturation is shown in green, undersaturation in purple and pink. Please note the different ranges of the colorbars. The boxes in the upper left graph indicate the locations of the Northern Channels (NC), Lake Isac (LI) and Canal Vatafu-Imputita (CVI).

4 DISCUSSION

4.1 From Patterns to Processes

The simultaneous analysis of different dissolved gas concentrations at high spatial resolution allows us to identify systematic patterns of concentration anomalies across the waterscapes of the Danube Delta. Comparing reactive with non-reactive gas concentrations, we identify relevant physical and biological processes such as excess air formation (Kipfer et al., 2002), ebullition (Brennwald et al., 2005; McGinnis et al., 2006) and ecosystem metabolism (Staehr et al., 2012). Two features in the concentration maps (Figures 3–5) deserve special attention. In the Eastern channels (Canal Busurca, Canal Rosu-Imputita and Canal Vatafu-Imputita; Figure 1) we observed hotspots of CH_4 and CO_2 concentrations (Figure 3). The clear oversaturation of non-reactive gases such as Ar and N_2 in this area could help us to identify potential drivers of these emission hotspots (Figures 4, 5). By contrast, the survey revealed a general under-saturation of dissolved CO_2 in lakes (Figure 3). Here, changes in diel O_2 concentrations could allow estimating the intensity of photosynthesis (Staehr et al., 2012). However, the observed under-saturation of He, Ar and N_2 (Figures 4, 5) points to a non-biological sink of dissolved gases that could affect primary production estimates based on O_2 concentrations.

A statistical display of the individual measurements in May and October reveals a broad distribution of measured values (Figure 6). The plot summarizes all data grouped according to waterscapes in the left panel, while the right-hand side presents only data from “boxed” areas in Figure 1: the Northern Channels, the hotspot channel Canal Vatafu-Imputita in the East and Lake Isac in the center of the study area. Part of the variability is caused by dramatic concentration changes at the local level (Figures 3, 5). The small channels in the vicinity of Canal Vatafu-Imputita are a case in point: here, the hydrology is characterized by stagnant conditions with very slow flow velocities. Sudden changes in discharge in the main river can even reverse the flow direction and introduce water from the Sulina main branch to an area that otherwise receives water from the delta. In contrast to the main branch, the water from the delta has a strong signature from the reed and elevated greenhouse gas concentrations. Therefore, dissolved gas concentrations of CO_2 , CH_4 and O_2 change abruptly along channel junctions. In the Northern Channels, the gradients were more gradual. There, larger concentration changes show a relation to channel junctions. We observed similar broad concentration shifts in lakes such as Lake Isac. Here, greenhouse gas concentrations were highest in the East, where water was entering from a small connecting channel with Canal Litcov and from riparian reed beds. O_2 showed the opposite trend with lowest concentrations in

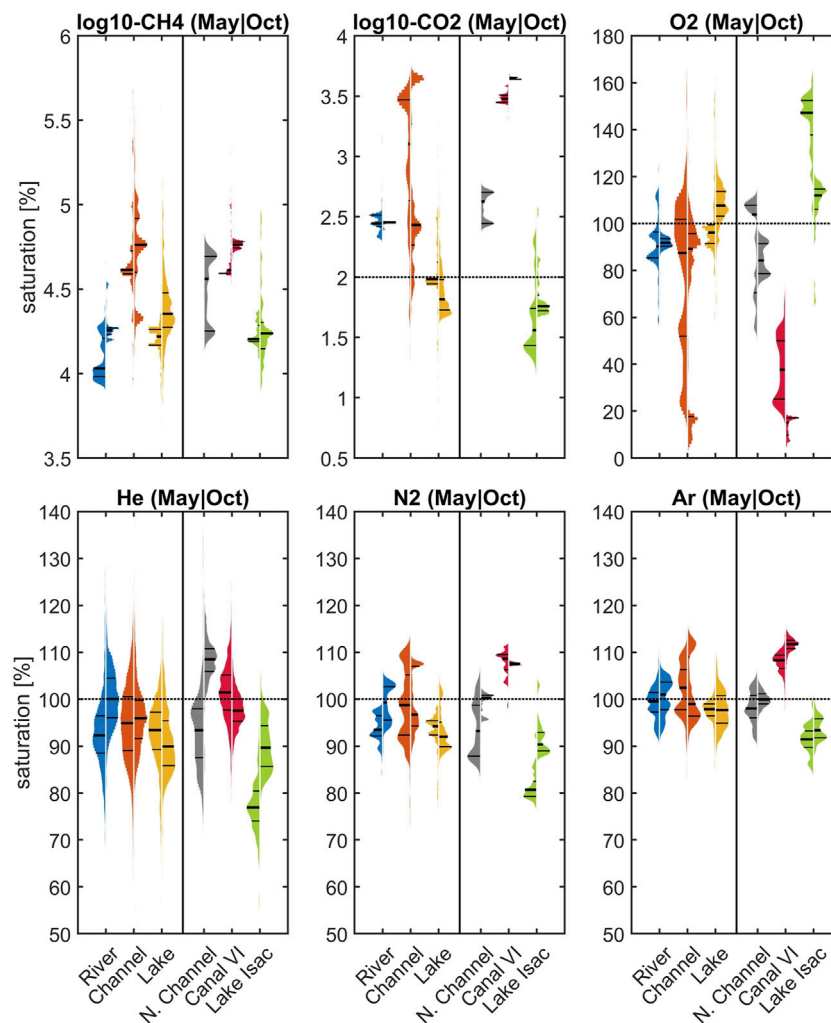


FIGURE 6 | Variability in CH_4 , CO_2 , O_2 , He, N_2 and Ar saturations with respect to different waterscapes (river, channel, lake) and three selected areas in May (left distribution) and October (distribution on the right). Horizontal lines in the distributions mark the 25th, 50th and 75th percentile. Horizontal dotted lines represent 100% saturation. In case of CH_4 this line is below the selected plotted area. Please note the different scaling of the y-axis and the representation of CH_4 and CO_2 as $\log_{10}()$. See boxes in **Figure 1** for the location of the specific areas Northern Channels, Canal Vatafu-Imputita and Lake Isac and **Supplementary Tables S3 and S4**.

the East. Wind-driven gas exchange drove re-equilibration and therefore, the dissolved gas signatures supplied by the lakes to the outflow channels changed gradually with increasing distance from the lake source.

The comparison of dissolved gas patterns across waterscapes yields valuable diagnostic insights (**Figure 6**). Focusing on non-reactive gases, the reaches of the Danube River remained close to saturation, whereas parts of the channels and most prominently Canal Vatafu-Imputita remained clearly oversaturated with respect to Ar and N_2 during both seasons. Therefore, an effective mechanism of excess air formation seems to be present in some of the small channels that form hot spots of potential greenhouse gas emissions. By contrast, lakes in general, and especially Lake Isac, showed a tendency towards undersaturation in their non-reactive gas concentrations. This undersaturation in He and N_2 in Lake Isac was more pronounced in May (77 and 81% for He and N_2 , respectively) compared to

October (~90% for both He and N_2) and indicates that a stripping mechanism is active in the transfer of unreactive gases to the atmosphere.

As expected, the O_2 and CO_2 patterns revealed heterotrophic characteristics of the main branches of the Danube River (**Figure 6**) with oversaturation of CO_2 and general O_2 deficits. The channels showed the same heterotrophic pattern but with a very broad distribution that could potentially be traced to their interaction with the littoral zone and the reed beds. Lake Isac, by contrast, showed evidence for intense photosynthesis in the summer, with around 150% O_2 saturation and lower autotrophy in October with about 110% O_2 .

To discuss possible sources and sinks of unreactive gases, we will address a few hypotheses that could help identifying the role of different physical processes in generating the observed patterns in the Danube Delta (**Figure 7**). In the context of excess air in channels, several studies documented the role of water table

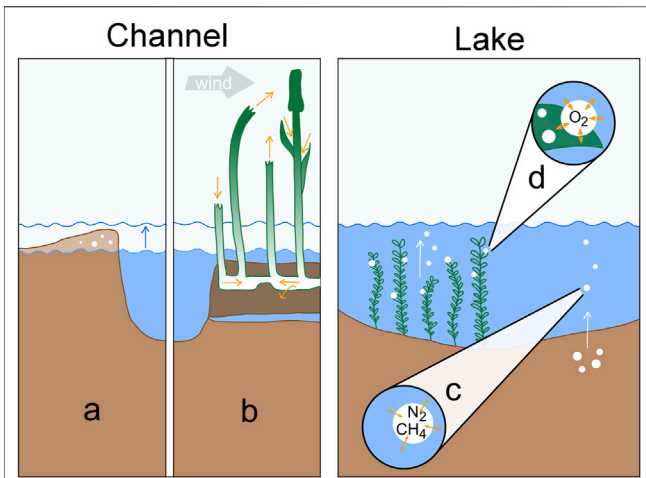


FIGURE 7 | Processes determining dissolved gas concentrations in channels (left) and shallow lakes (right): **(A)** Excess air formation via water table fluctuation in riverbanks. **(B)** Convective sediment aeration by *Phragmites australis* in permanently inundated reed areas. The two left culms illustrate venturi-induced convection, the right two culms represent humidity-induced convection. **(C)** Gas stripping by CH_4 bubbles rising from anoxic sediments. **(D)** Gas stripping by O_2 bubbles forming on macrophyte leaves during intensive photosynthesis.

fluctuations in unconfined groundwater bodies (e.g., Kipfer et al., 2002; Mächler et al., 2013). In the Eastern Danube Delta, however, floating reed vegetation is a much more prominent feature of the littoral zone than sand bars or riparian soils, which calls for another supersaturation formation hypothesis. In lakes, the release of methane bubbles at the sediment-water interface could drive gas ebullition to the atmosphere and result in dissolved gas deficits (McGinnis et al., 2006). Alternatively, accumulating oxygen bubbles at the surface of submerged macrophytes would provide an additional pathway for the loss of unreactive gases in the water column (Long et al., 2020).

4.2 Excess Air Is Tracing Emission Hotspots Near Reed Beds

The solubility of gases decreases with increasing temperature. The temperature sensitivity of this equilibrium process varies between different gases (Figure 8). While the solubility of He decreases by about 6% when the water temperature increases from 10 to 30°C, Ar solubility will diminish by 33%. This contrasting behavior can be used to estimate the amount of excess air, i.e., the excess in dissolved atmospheric gases, caused by dissolving air bubbles in water. Plotting the data from our surveys in Figure 8 reveals significant excess air components in the samples of Canal Vatafu-

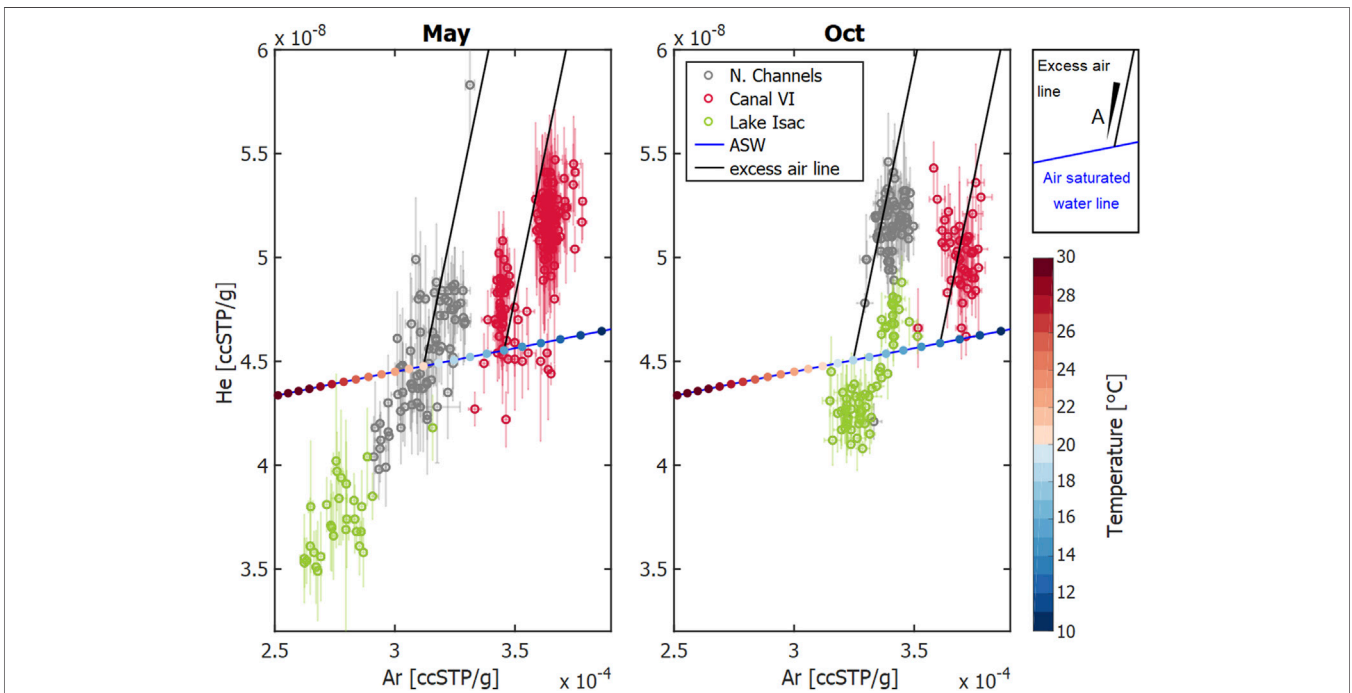


FIGURE 8 | He vs. Ar concentration in ccSPT/g, i.e., cubic centimeter of gas at standard pressure and temperature per gram of water in samples from the indicated locations in May and October 2017. The open circles show the average data from different observation sites, standard deviations are shown as error bars. The blue lines represent the concentrations in air-saturated water (ASW) at different temperatures; with temperature in °C represented as color-coded dots at 1°C increments. The solid black lines represent the excess-air lines for temperatures that fit well with the measured data: T = 20°C and T = 15°C (May), and T = 18°C and T = 13°C (Oct). The amount of dissolved air, A, increases with increasing distance from the ASW line.

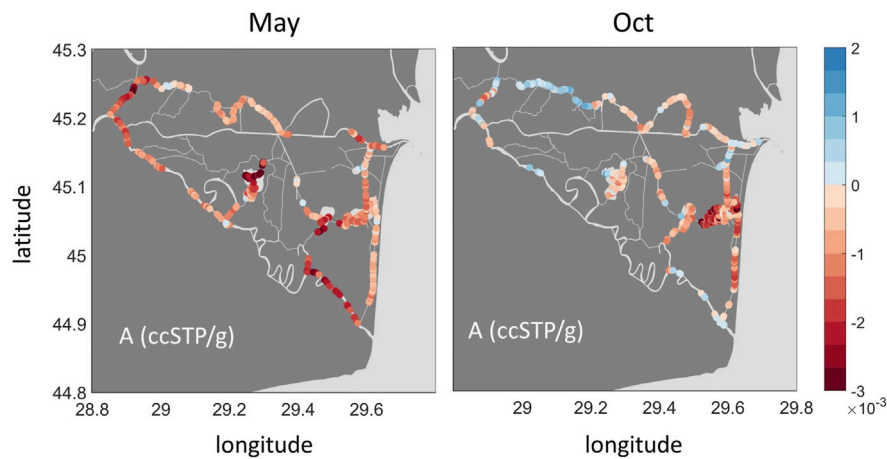


FIGURE 9 | Spatial variability in the estimates of excess air A for May (left) and October (right).

Imputita during both seasons, while the Northern Channels only show consistent excess air in October. The data from Lake Isac, by contrast, indicate significant gas loss (**Figure 8**).

Knowledge regarding the geomorphological and ecological context of the different sites helps in the identification of processes that cause the observed patterns in **Figure 8**. The Northern Channels are framed by riverbanks representing a potential setting for excess air formation via water table fluctuations (**Supplementary Figure S8**). During rising water table, entrapped bubbles in the unsaturated zone dissolve and increase local concentrations above saturation (Kipfer et al., 2002). Both campaigns in spring and autumn took place during falling water level (**Supplementary Figure S1**), when we expect previously enriched water to exfiltrate from the riverbanks back into the channels (**Figure 7A**). Once in the channel, gas exchange ensures re-equilibration of the oversaturated water with the atmosphere. In addition, tourist boats navigate the Northern Channels extensively from spring through summer and autumn, enhancing gas exchange, but defining a causal link would require time-resolved monitoring of excess air and boat traffic.

Canal Vatafu-Imputita, on the other hand, is situated in a depression zone framed by permanently inundated reed beds (**Supplementary Figure S8**). We were thus initially surprised to find supersaturated conditions at this location, especially since it is one of very few locations showing excess air in both seasons (**Figure 9**). While the excess air signal in October was comparable to the Northern Channels, the equilibration temperature was about 5°C lower (**Figure 8**; **Supplementary Figure S6**). As there are no adjacent riverbanks and rather little traffic at Canal Vatafu-Imputita, we found only two potential drivers for the excess air signal at this location: rapid heating or convective gas addition via reed vegetation.

As indicated by the difference between equilibrium temperature obtained from the UA-model and the *in-situ* measured temperature (**Supplementary Figure S7**), the equilibration could have taken place at an approximately 5°C lower temperature in the sun sheltered reed, with the water

parcel heating rapidly without changing its gas content once reaching the channel (**Supplementary Figure S4**). The channels within reed beds are rather wind sheltered environments as long as the main wind direction is perpendicular to the channel orientation. However, during sporadic measurements of daily temperature cycles in the channel, we only observed temperature fluctuations up to 2°C over the course of 1 day. Therefore, it seems unlikely that rapid heating would lead to the observed excess air signals.

We can therefore hypothesize that the plant physiology of the dominating reed species was the relevant cause of the oversaturation (**Figure 7B**). Equipped with aerenchyma (i.e., tissue with air channels, e.g., Baldantoni et al. (2009)), *Phragmites australis* transports O₂ in order to aerate its root zone (e.g., Brix et al., 1996). Aerating the root zone is vital for plants living in water logged or inundated soils, since anoxic sediment environments promote several adverse redox reactions (DeLaune and Reddy, 2008). The transportation mechanisms affect all gases present in air and wetland sediments (Sorrell and Brix, 2013). This way, He, Ar and N₂ are pumped into the root zone together with O₂ and could be used as tracers for plant-mediated oxygen supply.

Convective flow in plants is driven by a pressure gradient within the plant. The two most important gas transport processes in *Phragmites australis* are venturi-induced convection and humidity-induced convection (Armstrong et al., 1992). Venturi-induced flow is driven by wind blowing across the culms, thereby creating a pressure differential that sucks air out of tall dead culms. Short broken culms act as inflow and lead air along the underground root system to tall culms. The effectiveness of this process increases with wind speed (Armstrong et al., 1992). Humidity-induced flow works best during hot and dry days, since it relies on the pressure difference created by moistening of the air inside the plants living green shoots. Dead and broken culms act as efflux sites in this case (Armstrong et al., 1996). According to field measurements shortly above the water table, the pressure inside live culms is up to 2% higher than ambient air pressure

(Arkebauer et al., 2001). The exchange of gases between plant and rhizome is governed by diffusion (Armstrong et al., 1996).

Assuming the plants provide enough air to their root system to saturate the surrounding water with dissolved gases, we can estimate the level of noble gas oversaturation to be expected. The plaur which *Phragmites australis* grows on is about 0.8–1.3 m thick, so it is reasonable to assume that the root systems reach a depth of 1 m below water level. At this depth, the local hydrostatic pressure is about 10^4 Pa higher than atmospheric pressure. If the plants would provide enough air to this depth to saturate the water phase at this increased pressure, we would expect 10% oversaturation when comparing it to water equilibrated at local atmospheric pressure. This is approximately the amount of oversaturation we observed for He, Ar and N₂ in May and October in Canal Vatafu-Imputita (**Supplementary Figure S5**).

Based on field measurements, Brix et al. (1996) estimated the total gas exchange by *Phragmites australis* to 9–11 L m⁻² h⁻¹. Assuming an air-like gas composition in the gas transport system of the plant and a dissolution of 10% of the gas transported by the total flux observed by Brix et al. (1996), would mean that 1.5–3.5 h were sufficient to supply the amount of N₂ and Ar to the root systems needed to create the observed oversaturation.

If reed beds play a significant role in the injection of excess air and high concentrations of CH₄ and CO₂, then how can we explain the different patterns observed in the GHG and excess air maps (**Figures 3, 9**)? Canal Vatafu-Imputita drains a core protection zone of the Danube Delta Biosphere Reserve, which is populated by *Phragmites australis*, while other core zones generally protect other vegetation types. In the core zone, harvesting and burning of the reed is not permitted, thus we expect more dead and broken culms that can function as efflux culms for the convective flow in this area, together with more degradable organic matter. Brix et al. (1996) report 280 dead and 85 living culms per square meter in their study area. At sites that are harvested and burnt we would expect the ratio to be shifted towards living culms as dead culms are removed regularly, which might restrict sediment aeration. A functioning soil aeration results in the oxidation of reduced species near the root zone, e.g., oxidation of CH₄ produced during organic matter degradation to CO₂ (DeLaune and Reddy, 2008). Looking at the maps in **Figure 3**, the high ratio of CO₂ to CH₄ indicates that CH₄ oxidation could be an important process in Canal Vatafu-Imputita. This seems plausible, considering that biofilms inhabiting the root surfaces of *Phragmites australis* consist to about one-third of bacteria capable of oxidizing CH₄ (Faußer et al., 2012). This could explain the buildup of high CO₂ concentrations in the water phase below the floating plaur which subsequently drain into Canal Vatafu-Imputita. The adjacent Canal Rosu-Imputita is draining the buffer area, where reed harvesting is allowed within limits. It shows higher CH₄ and lower CO₂ concentrations than Canal Vatafu-Imputita, especially in spring. The oversaturation of Ar, N₂ and He is also less in this channel during the early growing season, which may indicate that nearby reed beds are managed and O₂ transfer during the early growing season is hampered, resulting in a reduced oxidation capacity in the root zone.

Once the supersaturated water reaches the channel, diffusive re-equilibration with the atmosphere would decrease the oversaturation towards equilibrium. Intense boat traffic would enhance gas exchange and ebullition could strip the gases even below equilibrium. A combination of these processes might explain the comparably low He saturations observed at Canal Vatafu-Imputita (**Figure 6**).

4.3 Gas Loss by Ebullition in Shallow Lakes

In contrast to the channels, we observed undersaturation of He, Ar and N₂ in the lakes, especially in Lake Isac. This coincided with a CO₂ undersaturation and an O₂ oversaturation. The undersaturation of He, Ar and N₂ indicates that gas stripping by ebullition affects the dissolved gas concentrations, since a rising bubble exchanges gas with the surrounding water column and thereby strips dissolved gases depending on their solubility (Brennwald et al., 2005; McGinnis et al., 2006). Accordingly, in Lake Isac the hardly soluble He showed the strongest undersaturation, followed by the more soluble N₂ and Ar (compare **Figures 2** and **6**). As O₂ and Ar exhibit similar solubilities, undersaturation of Ar indicates that O₂ must be affected by gas stripping. We calculated the effect on O₂ concentration via O₂:Ar ratios (**Eq. 4** and **Figure 10**). For oversaturated O₂ conditions in May, we found a linear relation with missing O_{2,dif} down to about 2.5 mg/L at 150% saturation.

Gas ebullition is the most likely cause for the observed oxygen deficit and there are two potential drivers of such a process: CH₄ ebullition from the sediment (**Figure 7C**) and O₂ ebullition from macrophyte leaves (**Figure 7D**). Evaluating the dataset from Maier et al. (2020) showed that CH₄ ebullition was most often present in lakes and channels, where it occurred in 43 and 42% cases of flux measurements around the year (Maier et al., 2020). However, with a depth of only about 1.5–4 m, the sampled delta lakes are comparably shallow (Oosterberg et al., 2000), which limits the contact time between water column and the rising gas bubble, thus restricting gas exchange (McGinnis et al., 2006). A pure CH₄ bubble with an initial size of 2 mm would still contain 70% of the initial CH₄ if released from 4 m depth. Larger bubble diameter or shallower release depth would increase the percentage of initially CH₄ transported (Greinert and McGinnis, 2009). CH₄ bubbles released from the sediment usually contain large amounts of N₂. Assuming the minimum amount of CH₄ needed to trigger the rise of a bubble through the sediment would result in an approximate CH₄:N₂ composition of 35:65% (Langenegger et al., 2019). A CH₄/N₂ bubble released in a lake with 2 m depth would transport on average about 5.3 μg O₂ per bubble to the atmosphere (**Supplementary Figure S10**). Thus, about 0.8 million methane bubbles per m² would have to be released to the atmosphere from a fully mixed water column of 2 m depth to account for the buildup of a daily oxygen deficit of 2 g m⁻³. This would equal a CH₄ flux of 3.1 mol m⁻² day⁻¹, which is about 60 times higher than the maximum total CH₄ flux measured in lakes and more than 2,000 times higher than the median total CH₄ flux from lakes in the Danube Delta (Maier et al., 2021). In the case of CH₄ ebullition being the sole cause of O₂ reduction, we would expect gas stripping to be strongest after macrophyte die-off or in autumn when large amounts of easily

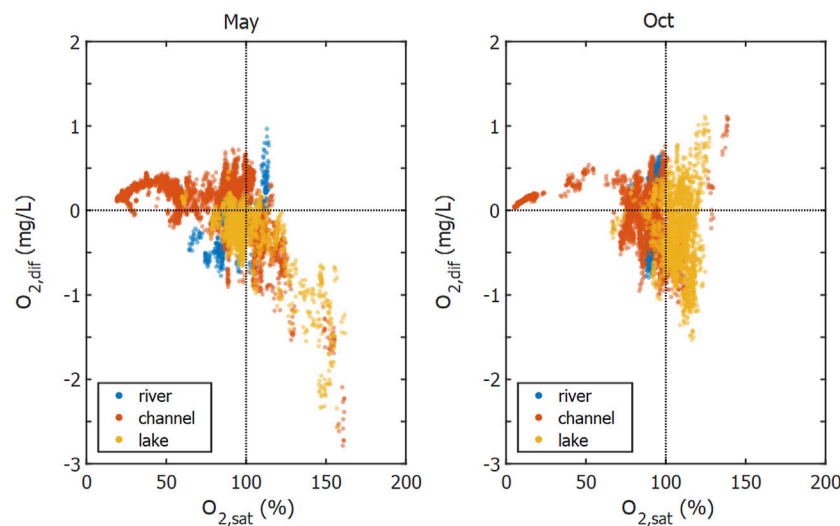


FIGURE 10 | O_2 concentration difference of O_2 calculated from $O_2:Ar$ ratio (Eq. 4). Color coding indicates the different waterscapes. Negative values of $O_{2,dif}$ occur for samples with significant undersaturation in the Ar concentration.

degradable material are available. Considering the large fluxes needed and the unusual timing, it is unlikely for CH_4 ebullition to be the dominant process reducing the saturation of dissolved gases in May and we therefore turn our attention to photosynthesis.

In spring, the bottom of Lake Isac was covered by macrophytes, many of them reaching close to the water surface (Supplementary Figure S11). If photosynthesis is very productive, bubbles containing N_2 and a lot of O_2 form on the leave surface of macrophytes and can be released via ebullition (Koschorreck et al., 2017). In contrast to CH_4 bubbles rising from the sediment, these O_2 bubbles spent considerably longer time in contact with the water column until they detach and rise to the surface. This process would also explain the quasi-linear relationship between observed oversaturation and estimated amount of missing O_2 , assuming that stronger oversaturation coincided with more O_2 bubble formation and increased release to the surface. Strong oversaturation together with missing O_2 was almost exclusively observed in the lakes (Supplementary Figure S9), especially in Lake Isac and Lake Puiu in spring where median O_2 saturation was 147 and 115%, respectively. Both lakes are also the sites where He and Ar saturations were lowest with median saturations of 76.9 and 91.4% in Lake Isac, and 87.5 and 96.9% in Lake Puiu, respectively. Temperature-corrected, specific conductivity was lower in these lakes than in the main river (Supplementary Figure S3). This may also indicate high primary productivity because intense photosynthesis takes up CO_2 , thus increasing pH, shifting the carbonate equilibrium, and leading to calcite precipitation and a decrease of specific conductivity (Dittrich et al., 2004; Ostrofsky and Miller, 2017).

The combined measurements of non-reactive gases and O_2 thus indicate that photosynthesis was even higher than indicated by *in-situ* O_2 oversaturation. Whether the inter-lake differences are caused by differences in submerged macrophyte abundance (Coops et al., 1999) or caused by differences in macrophyte

species (Niculescu et al., 2020) cannot be concluded without further research. In any case, the current findings support several recent studies that highlight the importance of considering ebullitive gas exchange when estimating metabolism from diel O_2 concentration measurements in shallow ecosystems and propose to constrain ebullition rates using funnels or modelling the gas exchange from noble gas measurements (Koschorreck et al., 2017; Howard et al., 2018; Long et al., 2020). The reduction of daily net O_2 production estimates by ebullitive O_2 fluxes is estimated to about 1–21% (Howard et al., 2018).

4.4 Implications for Process Analysis and Upscaling

High-resolution mapping of biogenic and inert dissolved gases across the waterscapes of the Danube Delta revealed a broad range in the saturation state of the greenhouse gases CO_2 and CH_4 (Figure 3). The main river reaches showed the expected behavior of a net heterotrophic ecosystem metabolism with slight supersaturation in both gases (Figure 6).

The channels in a delta system represent the reactive pipes transferring water from lakes and wetlands back into the main river and finally to the sea. Measuring the patterns of unreactive gases in channels provided additional insights: Signals of excess air in a canal close to floating natural *Phragmites* stands provided evidence for convective gas transfer into the root zone and for intensified CH_4 oxidation resulting in elevated levels of CO_2 at comparatively low CH_4 concentration. This preliminary assignment of most plausible processes to a set of dissolved gas patterns may help in guiding further research into the “black-box” of terrestrial-aquatic linkages at densely vegetated aquatic-terrestrial boundaries.

In comparison to the river reaches and channels, the shallow lakes were dominated by photosynthesis with clear CO_2 deficits and

O₂ oversaturation (Figures 3, 5). In these highly productive systems (Durisch-Kaiser et al., 2011; Maier et al., 2021), non-reactive gases gave clear evidence for O₂ ebullition from macrophytes, a process that deserves further attention. Ebullitive loss of O₂ to the atmosphere complicates the estimation of net ecosystem production in shallow lakes (Koschorreck et al., 2017), beds of macrophytes and with floating vegetation (Kleinschroth et al., 2021). Such plant communities in freshwater systems remain a significant challenge for efforts to upscale net CO₂ exchange.

The current discussion and global synthesis of the carbon transfer along the land-ocean aquatic continuum (LOAC, Regnier et al., 2013) is still dominated by active pipe models (Cole et al., 2007; Abril and Borges, 2019). Such a river engineering approach falls short of capturing the dramatic changes in the biomorphology of large river corridors of the last century. Surveys identified a loss of around 80% of the riparian wetlands in the lower Danube River corridor (Csagoly et al., 2016). On a global scale, preliminary estimates arrive at a loss of wetland area in the range of 17–50% between 1970 and 2008 depending on the region (Dixon et al., 2016). Loss or restoration of riparian wetland areas will certainly affect the greenhouse gas budgets of large river systems, but adequate measurements and models are needed to derive reliable estimates.

Based on this case study, we conclude, that adding non-reactive gas tracers to the toolbox of biogeochemical analysis offers significant potential for disentangling physical and biological processes in deltaic systems. Our analysis identifies root aeration of *Phragmites australis* reed beds as a plausible process leading to the oversaturation of small channels with non-reactive gas species as well as greenhouse gases. Furthermore, we highlight the effect of O₂ ebullition on dissolved gas concentrations in shallow lakes and the risk of underestimating metabolic rates derived from O₂ concentrations.

DATA AVAILABILITY STATEMENT

The datasets presented in this study can be found in the following online repositories: The data set with the MIMS measurements presented (i.e. He, Ar, O₂ and N₂) and accompanying metadata files are available via the ETH Research Collection at <https://doi.org/10.3929/ethz-b-000537695> (Maier et al., 2022). The CO₂, CH₄, temperature and conductivity data have been uploaded

REFERENCES

- Abril, G., and Borges, A. V. (2019). Ideas and Perspectives: Carbon Leaks from Flooded Land: Do We Need to Replumb the Inland Water Active Pipe? *Biogeosciences* 16 (3), 769–784. doi:10.5194/bg-16-769-2019
- Aeschbach-Hertig, W., El-Gamal, H., Wieser, M., and Palcsu, L. (2008). Modeling Excess Air and Degassing in Groundwater by Equilibrium Partitioning with a Gas Phase. *Water Resour. Res.* 44 (8), 1–12. doi:10.1029/2007wr006454
- Aeschbach-Hertig, W., Peeters, F., Beyerle, U., and Kipfer, R. (1999). Interpretation of Dissolved Atmospheric noble Gases in Natural Waters. *Water Resour. Res.* 35 (9), 2779–2792. doi:10.1029/1999wr900130
- Arkebauer, T. J., Chanton, J. P., Verma, S. B., and Kim, J. (2001). Field Measurements of Internal Pressurization in *Phragmites Australis* (Poaceae)

to PANGAEA, available at: <https://doi.pangaea.de/10.1594/PANGAEA.925080> (last access: 20.01.2021, Canning et al., 2020).

AUTHOR CONTRIBUTIONS

MSM, AC and BW conceptualized the present study. MSM, AC, CT and MB participated in field work. AC processed and analyzed the CO₂ and CH₄ data, MSM processed and analyzed the other dissolved gases. MSM conducted the excess air model calculations with support from MB. MSM prepared the figures, supplementary material, and, together with BW, drafted the manuscript. All authors engaged in discussing and editing the paper.

FUNDING

This work was supported by the Swiss State Secretariat for Education, Research and Innovation (SERI; grant no. 15.0068). The research leading to these results has received funding from the European Union's Horizon 2020 research and innovation program under the Marie Skłodowska-Curie Actions (grant no. 643052; C-CASCADES project).

ACKNOWLEDGMENTS

The authors thank Tim Kalvelage, Alexander Mistretta, Till Breitenmoser and our Romanian houseboat crew for their support during fieldwork. We thank the entire 4H- JENA team for their support with the CH₄ and CO₂ sensors, as well as Dan McGinnis and Rolf Kipfer for fruitful discussions and suggestions.

SUPPLEMENTARY MATERIAL

The Supplementary Material for this article can be found online at: <https://www.frontiersin.org/articles/10.3389/fenvs.2022.838126/full#supplementary-material>

and Implications for Regulation of Methane Emissions in a Midlatitude Prairie Wetland. *Am. J. Bot.* 88 (4), 653–658. doi:10.2307/2657065

Armstrong, J., Armstrong, W., Beckett, P. M., Halder, J. E., Lythe, S., Holt, R., et al. (1996). Pathways of Aeration and the Mechanisms and Beneficial Effects of Humidity- and Venturi-Induced Convections in *Phragmites Australis* (Cav.) Trin. Ex Steud. *Aquat. Bot.* 54 (2), 177–197. doi:10.1016/0304-3770(96)01044-3

Armstrong, J., Armstrong, W., and Beckett, P. M. (1992). *Phragmites Australis*: Venturi- and Humidity-Induced Pressure Flows Enhance Rhizome Aeration and Rhizosphere Oxidation. *New Phytol.* 120 (2), 197–207. doi:10.1111/j.1469-8137.1992.tb05655.x

Baldantoni, D., Ligrone, R., and Alfani, A. (2009). Macro- and Trace-Element Concentrations in Leaves and Roots of *Phragmites Australis* in a Volcanic lake in Southern Italy. *J. Geochemical Exploration* 101 (2), 166–174. doi:10.1016/j.gexplo.2008.06.007

- Battin, T. J., Kaplan, L. A., Findlay, S., Hopkinson, C. S., Marti, E., Packman, A. I., et al. (2008). Biophysical Controls on Organic Carbon Fluxes in Fluvial Networks. *Nat. Geosci* 1 (2), 95–100. doi:10.1038/ngeo101
- Bernhardt, E. S., Heffernan, J. B., Grimm, N. B., Stanley, E. H., Harvey, J. W., Arroita, M., et al. (2018). The Metabolic Regimes of Flowing Waters. *Limnology and Oceanography* 63, S99–S118. doi:10.1002/lno.10726
- Borges, A. V., and Abril, G. (2011). “Carbon Dioxide and Methane Dynamics in Estuaries,” in *Treatise on Estuarine and Coastal Science*. Editors E. Wolanski, and D. McLusky (Waltham: Academic Press), 119–161. doi:10.1016/b978-0-12-374711-2.00504-0
- Brennwald, M. S. (2020). *Noblefit - Quantitative Interpretation of Environmental Tracer Data* [Online]. GitHub.com. Available at: <https://github.com/brennmat/noblefit> (Accessed 05 29, 2021).
- Brennwald, M. S., Kipfer, R., and Imboden, D. M. (2005). Release of Gas Bubbles from lake Sediment Traced by noble Gas Isotopes in the Sediment Pore Water. *Earth Planet. Sci. Lett.* 235 (1), 31–44. doi:10.1016/j.epsl.2005.03.004
- Brennwald, M. S., Schmidt, M., Oser, J., and Kipfer, R. (2016). A Portable and Autonomous Mass Spectrometric System for On-Site Environmental Gas Analysis. *Environ. Sci. Technol.* 50 (24), 13455–13463. doi:10.1021/acs.est.6b03669
- Brix, H., Sorrell, B. K., and Schierup, H.-H. (1996). Gas Fluxes Achieved by *In Situ* Convective Flow in Phragmites Australis. *Aquat. Bot.* 54 (2), 151–163. doi:10.1016/0304-3770(96)01042-x
- Cai, W.-J. (2011). Estuarine and Coastal Ocean Carbon Paradox: CO₂ Sinks or Sites of Terrestrial Carbon Incineration? *Annu. Rev. Mar. Sci.* 3 (1), 123–145. doi:10.1146/annurev-marine-120709-142723
- Canning, A., Maier, M.-S., Wehrli, B., and Körtzinger, A. (2020). [Dataset]. Seasonal High-Resolution Sensor Data for pCO₂, pCH₄, O₂ and Temperature/salinity within the Danube Delta, Romania in 2017. Available at: <https://doi.pangaea.de/10.1594/PANGAEA.925080>. Accessed from 20 January, 2021.
- Canning, A. R., Fietzek, P., Rehder, G., and Körtzinger, A. (2021). Technical Note: Seamless Gas Measurements across the Land-Ocean Aquatic Continuum - Corrections and Evaluation of Sensor Data for CO₂, CH₄ and O₂ from Field Deployments in Contrasting Environments. *Biogeosciences* 18 (4), 1351–1373. doi:10.5194/bg-18-1351-2021
- Canning, A., Wehrli, B., and Körtzinger, A. (2021). Methane in the Danube Delta: the Importance of Spatial Patterns and Diel Cycles for Atmospheric Emission Estimates. *Biogeosciences* 18 (12), 3961–3979. doi:10.5194/bg-18-3961-2021
- Cole, J. J., Prairie, Y. T., Caraco, N. F., McDowell, W. H., Tranvik, L. J., Striegl, R. G., et al. (2007). Plumbing the Global Carbon Cycle: Integrating Inland Waters into the Terrestrial Carbon Budget. *Ecosystems* 10 (1), 171–184. doi:10.1007/s10021-006-9013-8
- Coops, H., Hanganu, J., Tudor, M., and Oosterberg, W. (1999). Classification of Danube Delta Lakes Based on Aquatic Vegetation and Turbidity. *Hydrobiologia* 415 (0), 187–191. doi:10.1007/978-94-017-0922-4_26
- Covaliov, S., Doroftei, M., and Hanganu, J. (2010). Danube Delta Biosphere Reserve (DDBR): Reef Dynamics within Actual Context. *Adv. Environ. Sci.* 2 (1), 69–79.
- Craig, H., and Hayward, T. (1987). Oxygen Supersaturation in the Ocean: Biological versus Physical Contributions. *Science* 235 (4785), 199–202. doi:10.1126/science.235.4785.199
- Csagoly, P., Magnin, G., and Hulea, O. (2016). “Lower Danube Green Corridor,” in *The Wetland Book: II: Distribution, Description and Conservation*. Editors C. M. Finlayson, G. R. Milton, R. C. Prentice, and N. C. Davidson. (Dordrecht: Springer Netherlands), 1–6. doi:10.1007/978-94-007-6173-5_251-1
- Deemer, B. R., Harrison, J. A., Li, S., Beaulieu, J. J., DelSontro, T., Barros, N., et al. (2016). Greenhouse Gas Emissions from Reservoir Water Surfaces: A New Global Synthesis. *BioScience* 66 (11), 949–964. doi:10.1093/biosci/biw117
- DeLaune, R. D., and Reddy, K. R. (2008). *Biogeochemistry of Wetlands: Science and Applications*. Boca Raton: CRC Press.
- DelSontro, T., Beaulieu, J. J., and Downing, J. A. (2018). Greenhouse Gas Emissions from Lakes and Impoundments: Upscaling in the Face of Global Change. *Limnol Oceanogr Lett.* 3 (3), 64–75. doi:10.1002/lol2.10073
- Dittrich, M., Kurz, P., and Wehrli, B. (2004). The Role of Autotrophic Picocyanobacteria in Calcite Precipitation in an Oligotrophic Lake. *Geomicrobiology J.* 21 (1), 45–53. doi:10.1080/01490450490253455
- Dixon, M. J. R., Loh, J., Davidson, N. C., Beltrame, C., Freeman, R., and Walpole, M. (2016). Tracking Global Change in Ecosystem Area: The Wetland Extent Trends index. *Biol. Conservation* 193, 27–35. doi:10.1016/j.biocon.2015.10.023
- Durisch-Kaiser, E., Doberer, A., Reutimann, J., Pavel, A., Balan, S., Radan, S., et al. (2011). Organic Matter Governs N and P Balance in Danube Delta Lakes. *Aquat. Sci.* 73 (1), 21–33. doi:10.1007/s00027-010-0156-5
- Faußer, A. C., Hoppert, M., Walther, P., and Kazda, M. (2012). Roots of the Wetland Plants *Typha Latifolia* and *Phragmites Australis* Are Inhabited by Methanotrophic Bacteria in Biofilms. *Flora - Morphol. Distribution, Funct. Ecol. Plants* 207 (11), 775–782. doi:10.1016/j.flora.2012.09.002
- Friedlingstein, P., O’Sullivan, M., Jones, M. W., Andrew, R. M., Hauck, J., Olsen, A., et al. (2020). Global Carbon Budget 2020. *Earth Syst. Sci. Data* 12 (4), 3269–3340. doi:10.5194/essd-12-3269-2020
- Garcia, H. E., and Gordon, L. I. (1992). Oxygen Solubility in Seawater: Better Fitting Equations. *Limnol. Oceanogr.* 37 (6), 1307–1312. doi:10.4319/lo.1992.37.6.1307
- Gastescu, P. (2013). *Map of the Danube Delta Biosphere Reserve*. 1:240000. Tulcea, Romania: Danube Delta Biosphere Reserve Authority DDBRA.
- Greiner, J., and McGinnis, D. F. (2009). Single Bubble Dissolution Model - the Graphical User Interface SiBu-GUI. *Environ. Model. Softw.* 24 (8), 1012–1013. doi:10.1016/j.envsoft.2008.12.011
- Groffman, P. M., Altabet, M. A., Böhlke, J. K., Butterbach-Bahl, K., David, M. B., Firestone, M. K., et al. (2006). Methods for Measuring Denitrification: Diverse Approaches to a Difficult Problem. *Ecol. Appl.* 16 (6), 2091–2122. doi:10.1890/1051-0761(2006)016[2091:mfmdda]2.0.co;2
- Hall, R. O., Tank, J. L., Baker, M. A., Rosi-Marshall, E. J., and Hotchkiss, E. R. (2016). Metabolism, Gas Exchange, and Carbon Spiraling in Rivers. *Ecosystems* 19 (1), 73–86. doi:10.1007/s10021-015-9918-1
- Hall, R. O., and Ulseth, A. J. (2020). Gas Exchange in Streams and Rivers. *WIREs Water* 7 (1), e1391. doi:10.1002/wat2.1391
- Hamme, R. C., and Emerson, S. R. (2004). The Solubility of Neon, Nitrogen and Argon in Distilled Water and Seawater. *Deep Sea Res. Oceanographic Res. Pap.* 51 (11), 1517–1528. doi:10.1016/j.dsr.2004.06.009
- Hanganu, J., Dubyna, D., Zhmud, E., Grigoras, I., Menke, U., Drost, H., et al. (2002). *Vegetation of the Biosphere Reserve “Danube Delta” - with Transboundary Vegetation Map on a 1:150000 Scale*. Romania, Ukraine and RIZA: Danube Delta National Institute, M.G. Kholodny - Institute of Botany & Danube Delta Biosphere Reserve The Netherlands. RIZA rapport 2002.049, Lelystad, ISBN 9036954797.
- Heaton, T. H. E., and Vogel, J. C. (1981). “Excess Air” in Groundwater. *J. Hydrol.* 50, 201–216. doi:10.1016/0022-1694(81)90070-6
- Holgerson, M. A., and Raymond, P. A. (2016). Large Contribution to Inland Water CO₂ and CH₄ Emissions from Very Small Ponds. *Nat. Geosci* 9 (3), 222–226. doi:10.1038/ngeo2654
- Horgby, Å., Canadell, M. B., Ulseth, A. J., Vennemann, T. W., and Battin, T. J. (2019). High-Resolution Spatial Sampling Identifies Groundwater as Driver of CO₂ Dynamics in an Alpine Stream Network. *J. Geophys. Res. Biogeosci.* 124 (7), 1961–1976. doi:10.1029/2019JG005047
- Howard, E. M., Forbrich, I., Giblin, A. E., Lott, D. E., III, Cahill, K. L., and Stanley, R. H. R. (2018). Using Noble Gases to Compare Parameterizations of Air-Water Gas Exchange and to Constrain Oxygen Losses by Ebullition in a Shallow Aquatic Environment. *J. Geophys. Res. Biogeosci.* 123 (9), 2711–2726. doi:10.1029/2018JG004441
- ICPDR (2019). [Dataset]. Danube River Basin Water Quality Database. Available at: <http://www.icpdr.org/wq-db/>. Accessed from 29 October, 2019.
- IPCC (2021). *Climate Change 2021: The Physical Science Basis*. Contribution of Working Group I to the Sixth Assessment Report of the Intergovernmental Panel on Climate Change. Cambridge University Press.
- Irimus, I. (2006). “The Hydrological Regime of the Danube in the Deltaic Sector,” in *Danube Delta: Genesis and Biodiversity*. (Editors C. Tudorancea and M. M. Tudorancea (Leiden, Netherlands: Backhuys Publishers), 53–64.
- Jonas (2021). Violin Plots for Plotting Multiple Distributions (distributionPlot.M) [Online]. Available at: <https://www.mathworks.com/matlabcentral/fileexchange/23661-violin-plots-for-plotting-multiple-distributions-distributionplot-m>. MATLAB Central File Exchange (Accessed January 17, 2021).
- Kipfer, R., Aeschbach-Hertig, W., Peeters, F., and Stute, M. (2002). Noble Gases in Lakes and Ground Waters. *Rev. Mineralogy Geochem.* 47 (1), 615–700. doi:10.2138/rmg.2002.47.14
- Kleinschroth, F., Winton, R. S., Calamita, E., Niggemann, F., Botter, M., Wehrli, B., et al. (2021). Living with Floating Vegetation Invasions. *Ambio* 50 (1), 125–137. doi:10.1007/s13280-020-01360-6

- Koschorreck, M., Hentschel, I., and Bohrer, B. (2017). Oxygen Ebullition from Lakes. *Geophys. Res. Lett.* 44 (18), 9372–9378. doi:10.1002/2017gl074591
- Langenegger, T., Vachon, D., Donis, D., and McGinnis, D. F. (2019). What the Bubble Knows: Lake Methane Dynamics Revealed by Sediment Gas Bubble Composition. *Limnol Oceanogr* 64 (4), 1526–1544. doi:10.1002/lno.11133
- Laruelle, G. G., Dürr, H. H., Slomp, C. P., and Borges, A. V. (2010). Evaluation of Sinks and Sources of CO₂ in the Global Coastal Ocean Using a Spatially-Explicit Typology of Estuaries and continental Shelves. *Geophys. Res. Lett.* 37 (15), L15607(1–6). doi:10.1029/2010gl043691
- Lauerwald, R., Laruelle, G. G., Hartmann, J., Ciais, P., and Regnier, P. A. G. (2015). Spatial Patterns in CO₂ evasion from the Global River Network. *Glob. Biogeochem. Cycles* 29 (5), 534–554. doi:10.1002/2014gb004941
- Long, M. H., Sutherland, K., Wankel, S. D., Burdige, D. J., and Zimmerman, R. C. (2020). Ebullition of Oxygen from Seagrasses under Supersaturated Conditions. *Limnol Oceanogr* 65 (2), 314–324. doi:10.1002/lno.11299
- Mächler, L., Peter, S., Brennwald, M. S., and Kipfer, R. (2013). Excess Air Formation as a Mechanism for Delivering Oxygen to Groundwater. *Water Resour. Res.* 49 (10), 6847–6856. doi:10.1002/wrcr.20547
- Maier, M.-S., Teodoru, C. R., and Wehrli, B. (2021). Spatio-temporal Variations in Lateral and Atmospheric Carbon Fluxes from the Danube Delta. *Biogeosciences* 18 (4), 1417–1437. doi:10.5194/bg-18-1417-2021
- Maier, M.-S., Teodoru, C. R., and Wehrli, B. (2020). [Dataset]. “Spatio-temporal Variations of Lateral and Atmospheric Carbon Fluxes from the Danube Delta (Dataset),” in *A 2-year Dataset of Measured Concentrations and Fluxes* (ETH Zurich). Available at: <http://hdl.handle.net/20.500.11850/416925>. doi:10.3929/ethz-b-000416925
- mapcruzin (2016). Mapcruzin.com [Online]. Available at: <https://mapcruzin.com/free-romania-arcgis-maps-shapefiles.htmwww.openstreetmap.org/> (Accessed 12 13, 2016).
- McGinnis, D. F., Bilsley, N., Schmidt, M., Fietzek, P., Bodmer, P., Premke, K., et al. (2016). Deconstructing Methane Emissions from a Small Northern European River: Hydrodynamics and Temperature as Key Drivers. *Environ. Sci. Technol.* 50 (21), 11680–11687. doi:10.1021/acs.est.6b03268
- McGinnis, D. F., Greinert, J., Artemov, Y., Beaubien, S., and Wüest, A. (2006). Fate of Rising Methane Bubbles in Stratified Waters: How Much Methane Reaches the Atmosphere? *J. Geophys. Res. Oceans* 111 (C9), C09007(1–15). doi:10.1029/2005JC003183
- Natchimuthu, S., Sundgren, I., Gålfalk, M., Klemedtsson, L., Crill, P., Danielsson, Å., et al. (2016). Spatio-temporal Variability of lake CH₄ Fluxes and its Influence on Annual Whole lake Emission Estimates. *Limnol. Oceanogr.* 61 (S1), S13–S26. doi:10.1002/lno.10222
- Niculescu, S., Boissonnat, J.-B., Lardeux, C., Roberts, D., Hanganu, J., Billey, A., et al. (2020). Synergy of High-Resolution Radar and Optical Images Satellite for Identification and Mapping of Wetland Macrophytes on the Danube Delta. *Remote Sensing* 12 (14), 2188. doi:10.3390/rs12142188
- Oosterberg, W., Staras, M., Bogdan, L., Buijse, A. D., Constantinescu, A., Coops, H., et al. (2000). *Ecological Gradients in the Danube Delta Lakes: Present State and Man-Induced Changes*. Lelystad: RIZA the Netherlands, Danube Delta Natinal Institute Romania and Danube Delta Biosphere Reserve Authority Romania. RIZA rapport nr. 2000.015.
- Ostrowsky, M. L., and Miller, C. (2017). Photosynthetically-mediated Calcite and Phosphorus Precipitation by Submersed Aquatic Vascular Plants in Lake Pleasant, Pennsylvania. *Aquat. Bot.* 143, 36–40. doi:10.1016/j.aquabot.2017.09.002
- Panin, N. (1996). Danube Delta - Genesis, Evolution and Sedimentology. *Geo-Eco-Marina* 1, 11–34.
- Pavel, A., Durisch-Kaiser, E., Balan, S., Radan, S., Sobek, S., and Wehrli, B. (2009). Sources and Emission of Greenhouse Gases in Danube Delta Lakes. *Environ. Sci. Pollut. Res. Int.* 16 Suppl 1 (1), S86–S91. doi:10.1007/s11356-009-0182-9
- Raymond, P. A., Hartmann, J., Lauerwald, R., Sobek, S., McDonald, C., Hoover, M., et al. (2013). Global Carbon Dioxide Emissions from Inland Waters. *Nature* 503 (7476), 355–359. doi:10.1038/nature12760
- Regnier, P., Friedlingstein, P., Ciais, P., Mackenzie, F. T., Gruber, N., Janssens, I. A., et al. (2013). Anthropogenic Perturbation of the Carbon Fluxes from Land to Ocean. *Nat. Geosci* 6, 597–607. doi:10.1038/ngeo1830
- Sachs, N. M. (2019). The Paris Agreement in the 2020s: Breakdown or Breakup. *Ecol. LQ* 46, 865. doi:10.15779/Z38H708140
- Sorrell, B. K., and Brix, H. (2013). “Gas Transport and Exchange through Wetland Plant Aerenchyma,” in *Methods in Biogeochemistry of Wetlands*. Editors R. DeLaune, K. Reddy, C. Richardson, and J. Magonigal (Madison WI: Soil Science Society of America), 177–196.
- Staehr, P. A., Testa, J. M., Kemp, W. M., Cole, J. J., Sand-Jensen, K., and Smith, S. V. (2012). The Metabolism of Aquatic Ecosystems: History, Applications, and Future Challenges. *Aquat. Sci.* 74 (1), 15–29. doi:10.1007/s00027-011-0199-2
- Stanley, E. H., Casson, N. J., Christel, S. T., Crawford, J. T., Loken, L. C., and Oliver, S. K. (2016). The Ecology of Methane in Streams and Rivers: Patterns, Controls, and Global Significance. *Ecol. Monogr.* 86 (2), 146–171. doi:10.1890/15-1027
- Tortell, P. D., Bittig, H. C., Körtzinger, A., Jones, E. M., and Hoppema, M. (2015). Biological and Physical Controls on N₂, O₂, and CO₂ distributions in Contrasting Southern Ocean Surface Waters. *Glob. Biogeochem. Cycles* 29 (7), 994–1013. doi:10.1002/2014GB004975
- Ulseth, A. J., Hall, R. O., Boix Canadell, M., Madinger, H. L., Niayifar, A., and Battin, T. J. (2019). Distinct Air-Water Gas Exchange Regimes in Low- and High-Energy Streams. *Nat. Geosci.* 12 (4), 259–263. doi:10.1038/s41561-019-0324-8
- UNEP-WCMC (UN Environment Programme World Conservation Monitoring Centre) (2021). World Heritage Datasheet - Danube Delta [Online]. Available at: <http://world-heritage-datasheets.unep-wcmc.org/datasheet/output/site/danube-delta/> (Accessed 07 27, 2021).
- UNESCO (2021). Ecological Sciences for Sustainable Development. Danube Delta. [Online]. Available at: <http://www.unesco.org/new/en/natural-sciences/environment/ecological-sciences/biosphere-reserves/europe-north-america/romaniaukraine/danube-delta/> (Accessed 07 26, 2021).
- Weiss, R. F. (1974). Carbon Dioxide in Water and Seawater: the Solubility of a Non-ideal Gas. *Mar. Chem.* 2 (3), 203–215. doi:10.1016/0304-4203(74)90015-2
- Weiss, R. F. (1971). Solubility of Helium and Neon in Water and Seawater. *J. Chem. Eng. Data* 16 (2), 235–241. doi:10.1021/je60049a019
- Wiesenburg, D. A., and Guinasso, N. L., Jr (1979). Equilibrium Solubilities of Methane, Carbon Monoxide, and Hydrogen in Water and Sea Water. *J. Chem. Eng. Data* 24 (4), 356–360. doi:10.1021/je60083a006
- Zhou, J., Delille, B., Brabant, F., and Tison, J.-L. (2014). Insights into Oxygen Transport and Net Community Production in Sea Ice from Oxygen, Nitrogen and Argon Concentrations. *Biogeosciences* 11 (18), 5007–5020. doi:10.5194/bg-11-5007-2014

Conflict of Interest: The authors declare that the research was conducted in the absence of any commercial or financial relationships that could be construed as a potential conflict of interest.

Publisher’s Note: All claims expressed in this article are solely those of the authors and do not necessarily represent those of their affiliated organizations, or those of the publisher, the editors and the reviewers. Any product that may be evaluated in this article, or claim that may be made by its manufacturer, is not guaranteed or endorsed by the publisher.

Copyright © 2022 Maier, Canning, Brennwald, Teodoru and Wehrli. This is an open-access article distributed under the terms of the Creative Commons Attribution License (CC BY). The use, distribution or reproduction in other forums is permitted, provided the original author(s) and the copyright owner(s) are credited and that the original publication in this journal is cited, in accordance with accepted academic practice. No use, distribution or reproduction is permitted which does not comply with these terms.